Renewable Energy 221 (2024) 119675

Contents lists available at ScienceDirect

Renewable Energy

journal homepage: www.elsevier.com/locate/renene

Constructing the large-scale collimating solar simulator with a light half-divergence angle <1° using only collimating radiation modules

Yuan Gao, Xuan Zhu, Jiangfeng Chen, Yin Xie, Jianan Hong, Junyu Jin, Junchou Han, Xuhan Zhang, Chenyu Xu [**], Yanwei Zhang [*]

State Key Laboratory of Clean Energy Utilization, Zhejiang University, Hangzhou, 310027, China

ARTICLE INFO

Keywords:
Collimating solar simulator
Large scale
Divergence angle
Collimation
Energy efficiency
Cost

ABSTRACT

Large-scale collimating solar simulators (CSSs) with a light half divergence angle (HDA) of less than 1° have been developed. The small HDA ensures that the CSS can effectively simulate the optical behavior between natural sunlight and optical devices. However, the construction of large-scale CSSs still has a strict threshold because additional optical modules (AOMs), such as large-area collimating mirrors, are usually required to correct the light into collimated light. The manufacturing, installation, and adjustment of these precision optical devices pose significant challenges. An excellent scheme to avoid AOMs is to use the collimating radiation module (CRM), which can directly produce collimated light. Unfortunately, CRM can only produce light with an HDA of more than 3° at present, far larger than that of CSS with AOMs. Here, we report a CRM that can directly produce light with excellent collimation (an HDA<0.955°) and uniformity (>90 %). We accomplished this by analyzing the deviations between an idealized geometric optical model and actual CRMs and eliminating them with high-precision parts and a high-resolution adjustment method. We further used 24 CRMs to prove that the single-module collimating solar simulator (SMCSS, a radiation area of 2.55 m × 1.57 m) could be modularly constructed by them. Experimental investigations involving light-concentrating experiments on a parabolic trough collector demonstrated the superior collimation and simulation capabilities of the SMCSS. By eliminating the need for AOMs, the CRM and SMCSS significantly reduce system complexity and cost and lower the construction threshold for large-scale CSSs. It will benefit all experimental scenarios that need large-area collimated light and greatly promote the application of large-scale CSS in civilian solar research.

1. Introduction

Solar simulators, instead of natural sunlight, are chosen as the light source in most studies on solar energy because they are more stable, quantitative, and repeatable [1]. Solar simulators can be divided into two basic categories: concentrating solar simulators and collimating solar simulators. Most reported solar simulators are concentrating simulators [2–4] that can produce a high-flux radiation spot by focusing light with ellipsoidal reflectors (Fig. 1a), directly providing the required radiative flux for experiments. On the other hand, the collimating solar simulators (CSSs) aim to produce uniformly collimated light to simulate natural sunlight.

They are used for simulating the sunlight-concentrating process to optimize the design of optical components in solar energy utilization systems, such as absorbers [5–8], reflectors [9–11], and secondary reflectors [12,13]. One of the core parameters of CSS is the half divergence angle (HDA) of light. An HDA closer to that of natural sunlight (0.267°) represents a better simulation effect. At present, some CSSs have achieved an HDA of less than 1° (Table 1).

However, the construction of large-scale CSSs is still challenging because most of them adopt multi-module configurations for small HDAs (Fig. 1b). Specifically, the radiation module produces concentrated light of a large HDA. Homogenization and collimation modules, such as optical integrators and collimating mirrors, are needed to correct the light to be collimated and uniform (Lines No.1-5 in Table 1) [16]. However, the two additional optical modules (AOMs) are the main obstacles to constructing large-scale CSSs. For instance, the collimation module usually uses a large-scale collimating mirror of the same area as the radiation area of the CSS. Nevertheless, its fabrication difficulty and cost increase exponentially with the area as a precise optical device,

* Corresponding author.
** Corresponding author.
E-mail addresses: mrxcy@zju.edu.cn (C. Xu), zhangyw@zju.edu.cn (Y. Zhang).

https://doi.org/10.1016/j.renene.2023.119675
Received 25 May 2023; Received in revised form 28 October 2023; Accepted 15 November 2023
Available online 11 December 2023

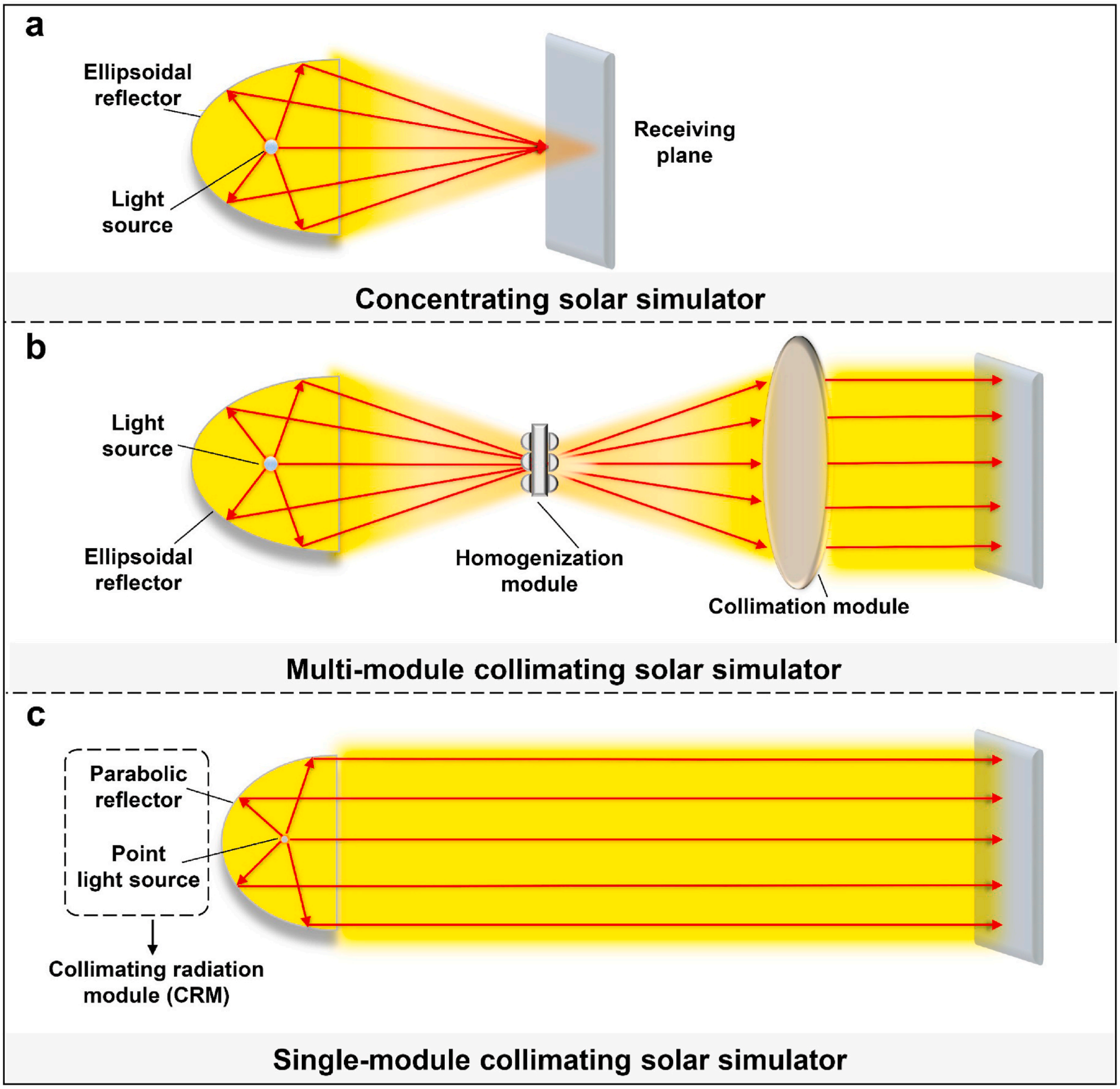

Fig. 1. Three kinds of solar simulators. (a) Concentrating solar simulator. (b) Multi-module collimating solar simulator. (c) Single-module collimating solar simulator.

Table 1
Parameters of the existing collimating solar simulators.

No.	Energy efficiency	Light source	HDA	Radiative flux (kW/m2)	Collimation module[b]	Homogenizing module[b]	Ref.
1	4.52 %	1 × 10 kW	<3.8°	6.40	Y	Y	[14]
2[a]	8.14 %	7 × 25 kW	~2°	1.4	Y	Y	[15]
3	9.88 %	37 × 20 kW	~1°	3.30	Y	Y	[16]
4	16.1 %	7 × 7 kW	<1.3°	0.94	Y	Y	[17]
5	16.2 %	19 × 20 kW	~3°	0.07–2.60	Y	Y	[16]
6	11.5 %	28 × 1 kW	~10°	1.08	N	N	[18]
7	31.6 %	24 × 3 kW	<0.955°	>13.00	N	N	This work

[a] A solar simulator at the Jet Propulsion Laboratory.
[b] Y and N represent the presence or absence of the module in the simulator, respectively.

whether directly manufactured or stitched with hundreds of spherical mirrors. The difficulty and cost may be acceptable when CSS is applied to outer space simulation in the early stage [14], but it hinders the further promotion of large-scale CSS in increasingly civil solar research today. In addition to their complexity and cost, AOMs also lead to the low energy efficiency of CSS (<20 %, Table 1) because of their interaction with light, so the high-power light sources and corresponding cooling equipment are always necessary, which further increases the system complexity.

An effective way to solve the disadvantage of multi-module collimating solar simulators (MMCSS) is to develop collimating radiation modules (CRMs) that can directly produce collimated light without AOMs (Line No.6 in Table 1) [18]. However, to our knowledge, the best CRM yet reported cannot produce light with an HDA of less than 3° [14],

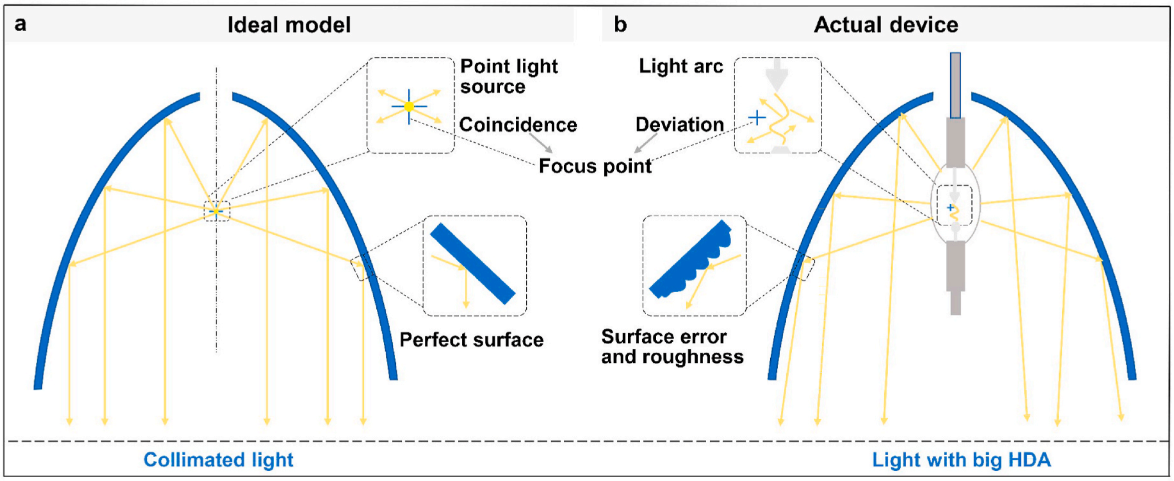

Fig. 2. Collimating radiation module. (a) Ideal model. (b) Actual device.

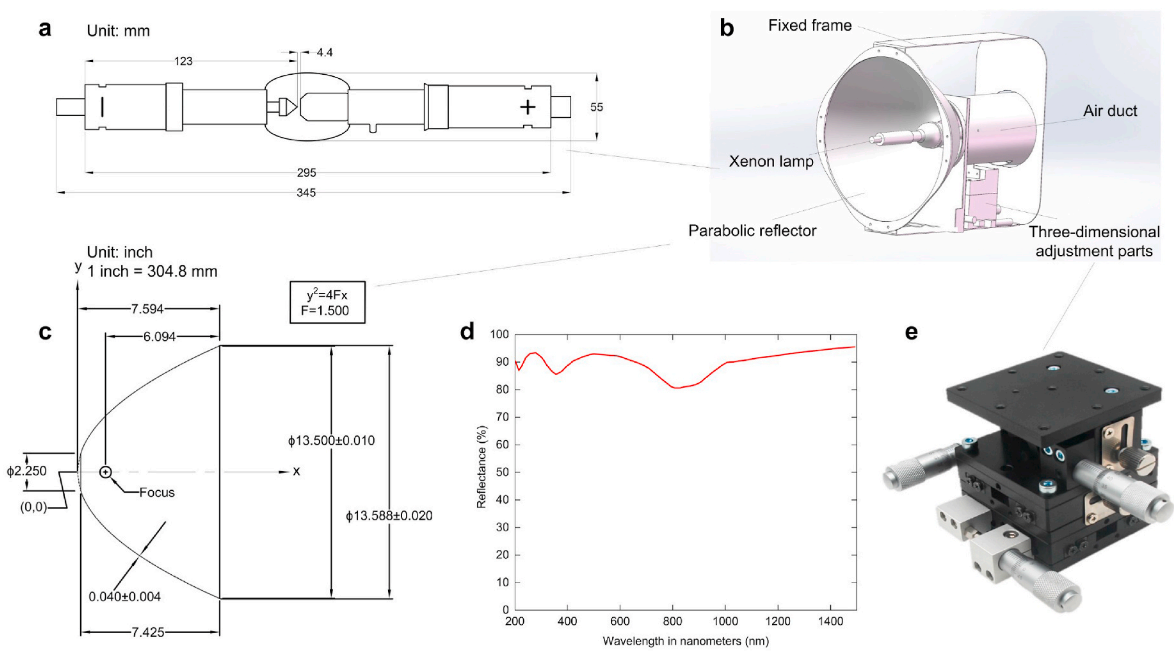

Fig. 3. Parts and the assembled CRM: **(a)** short-arc xenon lamp, **(b)** assembled CRM, **(c)** high-precision parabolic reflector, **(d)** change in reflectance of the reflector with wavelength, and **(e)** high-resolution three-dimensional adjustment parts.

much larger than that of CSS with AOMs. In this study, we achieved CRM with an HDA of less than 1° for the first time. We accomplished this by analyzing deviations between an idealized optical model (Figs. 1c and 2a) and actual CRMs and eliminating them with high-precision parts and a high-resolution adjustment method. More importantly, we proved that CRMs can modularly build large-scale single-module collimating solar simulators (SMCSSs) and successfully built an SMCSS composed of 24 CRMs with a radiation area of 2.55 m × 1.57 m. Light-concentrating experiments on a parabolic trough solar collector proved its excellent collimation and simulation capability.

2. Collimating radiation module (CRM)

2.1. Deviations between ideal model and actual CRMs

The theoretical basis of our CRMs is the idealized geometric optical model shown in Fig. 2a. When a point light source is placed at the focal point of a parabolic reflector, its light can be reflected into collimated light. This is a simple principle of geometric optics, and some simulation studies have proven the feasibility of realizing CRM with this principle [19]. However, only light with an HDA of larger than 3° could be obtained when turning the principle into a real device [14]. As Fig. 2b shows, we reasoned that three deviations cause the vast difference between the actual device and the ideal model: (a) the light source in a lamp is typically a light arc instead of a point. (b) The reflector has surface errors and roughness instead of being perfect. (c) The light arc cannot be placed strictly at the focal point of the reflector upon installation. Based on the analysis, our idea to realize the CRMs with this optical principle is to eliminate the gap between actual parts and the ideal model as much as possible from three aspects.

2.2. Design of the CRM to eliminate deviations

To eliminate the three deviation factors between the actual device and the ideal model, we use high-precision light sources and reflectors to get close to the ideal model, and a high-resolution three-dimensional

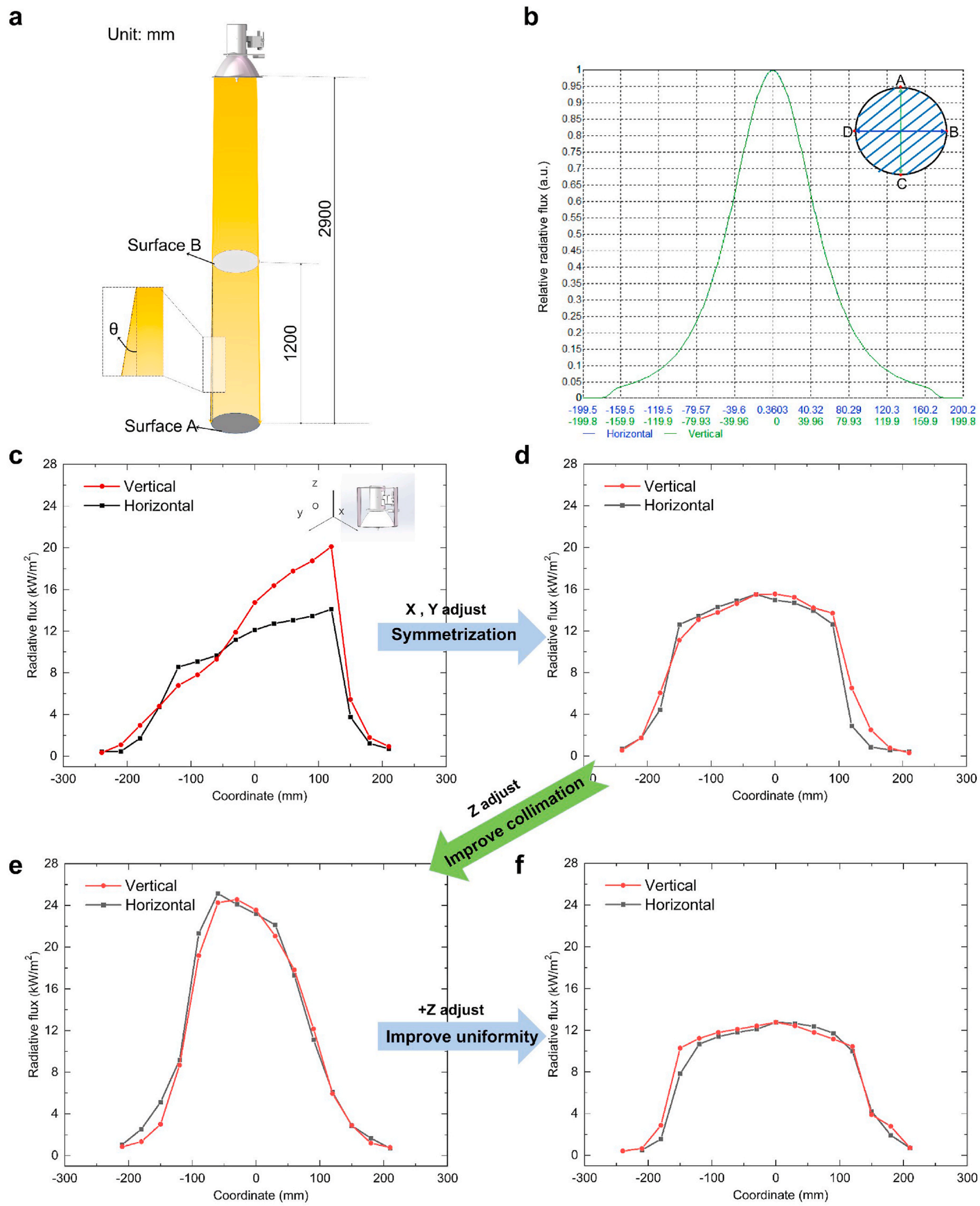

Fig. 4. (a) Light path of the CRM. **(b)** Simulated result of the radiation distribution of the ideal model, in which a point source is located at the focal point of a perfect parabolic reflector, and the radiative flux was normalized. The inset is a schematic diagram of the light spot, the radiation distribution was measured along diameter AC and BD. Radiation distribution changes in the adjustment process: **(c)** no adjustment, **(d)** after X- and Y-direction adjustment, **(e)** after Z-direction adjustment, and **(f)** further adjustment along the +Z direction. The three adjusting directions of the three-dimensional adjustment part are defined as X, Y, and Z directions, their relationship with the CRM is shown in the inset of (c).

method is also invented to adjust the relative position of the lamp and reflector to the optimum state. We selected a short-arc xenon lamp (XBO 3000 W/DHP OFR, OSRAM) [20] with a lamp arc length of only 4.4 mm to approach the point light source (Fig. 3a). The parabolic reflectors (P38-24, Optiforms) [21] were manufactured by electroforming to obtain high precision and repeatability (Fig. 3c). Nickel was deposited on the high-precision mandrel in the electroforming process, and the resulting error of the reflector inner surface was less than 2 arc minutes slope. Furthermore, an Al–SiO_2 thin film was fabricated on the surface of the reflector by vacuum deposition, which reduced the surface roughness to approximately 1.6 μm and provided high reflectivity in the visible and infrared regions (Fig. 3d). To precisely control the relative position of the light source and reflector, we installed three-dimensional adjustment parts (Fig. 3e) for the xenon lamps with an accuracy of 10 μm

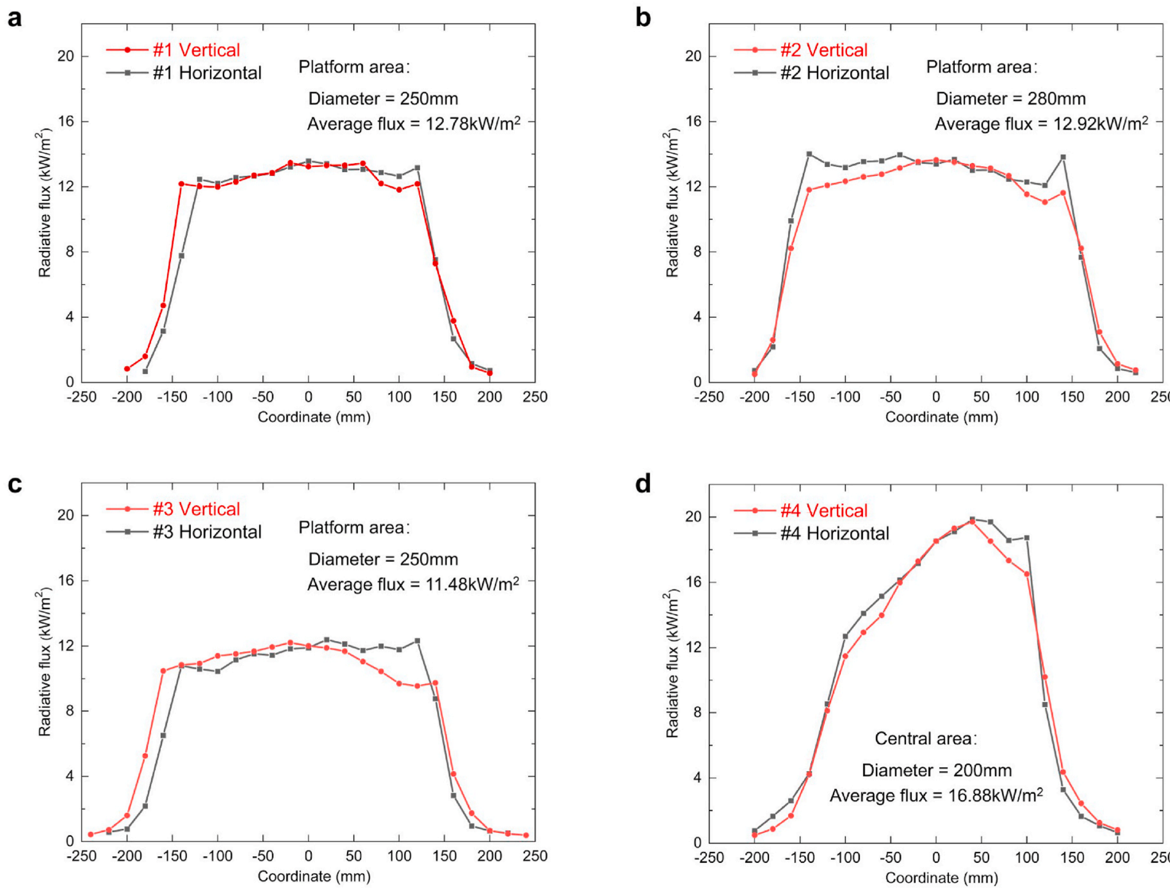

Fig. 5. Radiation distribution of **(a)** CRM #1, **(b)** CRM #2, **(c)** CRM #3, and **(d)** CRM #4, which were measured on a plane 2900 mm away from the light outlet of the CRMs. We calculated the diameter and average flux (Supplementary Note 3–4) of the platform area in the radiation distribution. The diameter and average flux of the central area were calculated with the same method for CRM #4 which does not include a platform area.

and an adjustment range of 10 mm. An optical power meter and a grid are used for measuring the radiation distribution to guide the adjustment.

2.3. Adjustment rules and repeatability of the CRM

Rules that adjust CRMs to obtain both excellent collimation and uniformity are studied. In the adjustment process, radiation distribution within the spot of the CRM was measured on surface A located on the ground (Fig. 4a). Thirty measurement points were evenly distributed on two perpendicular diameters of the spot (e.g. diameter AB and CD in the inset of Fig. 4b) to obtain radiative flux at the corresponding position. The initial radiation distribution (Fig. 4c) was not axisymmetric, and radiation distribution on two diameters is not consistent because the light arc of the lamp was not in the central axis of the reflector. The radiation distribution can become axisymmetric (Fig. 4d) by adjusting the lamp along the X and Y directions (the inset of Fig. 4c) to move the light arc to the central axis. Then, the lamp was adjusted along the Z direction to make the light arc closer to the focal point until a Gaussian-like distribution occurred (Fig. 4e). The Gaussian-like distribution represents excellent collimation because Monte Carlo ray tracing (MCRT) simulation proved that the ideal model (Fig. 2a) is also a Gaussian-like distribution (Fig. 4b, Supplementary Note 1). However, the Gaussian-like distribution has poor uniformity, which indicates that we might need to sacrifice a certain margin of collimation to optimize the uniformity. Therefore, the xenon lamp was adjusted along the +Z direction, the peak radiative flux significantly dropped, for example, a decrease of about 12 kW/m^2 (from Fig. 4e to f), and better uniformity was achieved. The adjustment process also demonstrated the necessity of a high-resolution adjustment method because the radiation flux distribution of CRMs is sensitive to adjustments. For example, we found that a 0.1 mm displacement of the lamp in the Z direction can cause a peak radiative flux change of approximately 5–6 kW/m^2. More quantitative details about the adjustment rules can be seen in Supplementary Note 2. Moreover, It should be noted that although collimation and uniformity have a trade-off relationship, both can be adjusted to excellent levels, which will be proven below.

The template method could be used in the adjustment of multiple CRMs to reduce workload (Supplementary Note 2), because the CRMs have outstanding repeatability that comes from the high precision of individual parts. Only five instead of thirty points need to be measured when adjusting a CRM with the template method, which greatly reduces the workload and is the significant basis of modularly constructing large-scale CSS. In Supplementary Note 2, we elaborated on how to obtain targeted radiation distribution with the template method.

2.4. Detailed study of HDA and uniformity

More experiments were conducted to prove that CRMs can obtain both excellent uniformity and small HDA. Four CRMs were adjusted with rules and the template method in section 2.3. CRM #1 (Fig. 5a) was adjusted as a template that sacrificed a degree margin of collimation to obtain higher uniformity, so there is an obvious platform area in its distribution. CRM #2, #3, and #4 were adjusted easily to obtain the target radiation distribution with CRM #1 as a template(Supplementary Note 2). #2, #3, and #4 respectively represent the cases that the target radiation distribution is consistent with the template, the average flux is lower, and the average flux is higher but the collimation is better.

Table 2
θ changes with the diameter difference of surfaces A and B (Δd).

Δd (mm)	0	10	20	30	40	50	60	70	80
θ (°)	0	0.239	0.477	0.716	0.955	1.19	1.43	1.67	1.91

Table 3
Measurement of HDA within surface A with a diameter of 200 mm.

CorrespondingHDA (°)		Power (W)			
		#1	#2	#3	#4
0°	Surface A, 200 mm	400.3	412.0	364.1	515.3
	Surface B, 200 mm	590.7	601.6	528.8	736.6
	Difference (%)	−47.6	−46.0	−45.2	−42.9
	Surface A, 200 mm	400.3	412.0	364.1	515.3
0.955°	Surface B, 160 mm	392.0	395.0	348.2	516.7
	Difference (%)	+2.1	+4.1	+4.4	−0.30

The uniformity of CRM #1 and #2 was calculated to be 94.1 % and 91.1 % in the platform area (Supplementary Note 3–4), respectively, which reached the C level (>90 %) of the solar simulator standard. It is remarkable that a radiation module without any homogenizing device, such as the optical integrator, can achieve uniformity of more than 90 %. This is undoubtedly due to the high accuracy of parts and adjustment methods.

For characterizing the collimation of the light, we measured the upper limit of the light HDA within the spot that is defined as θ_u. θ_u is measured based on two points: (1) We can measure the HDA of light on the edge of the spot, θ_e. (2) θ_u is equal to θ_e because we proved that the light closer to the center of the spot has a smaller HDA and better collimation, which will be proven later.

Therefore, the measurement of θ_e is core to measure θ_u of the spot. We achieved this with an indirect method by comparing optical power on two surfaces with a fixed distance. As shown in Fig. 4a, surface A and surface B had a fixed distance, and the diameter difference (Δd) of them determined an angle θ (Table 2). We decreased the diameter of surface B to increase θ in measurement. Smaller θ than θ_e (e.g. surface A and B have the same diameter and $\theta = 0°$) made surface A has lower optical power than surface B because the HDA of light decides that some light at the edge of surface B will not reach surface A after a 1.2 m propagation (Supplementary Fig. 4a). Larger θ than θ_e will lead to a higher power on surface A than surface B because some lights that do not pass surface B reach surface A (Supplementary Fig. 4c). The difference in optical power on two surfaces will be zero only if the θ is equal to θ_e (Supplementary Fig. 4b). Therefore, within the allowable range of error, we defined θ_e (equal to θ_u) is the θ when the difference of optical power on the two surfaces is less than 5 %.

The four CRMs were measured with the above method (Supplementary Note 4, Fig. 5, Supplementary Fig. 5), and their θ_u was

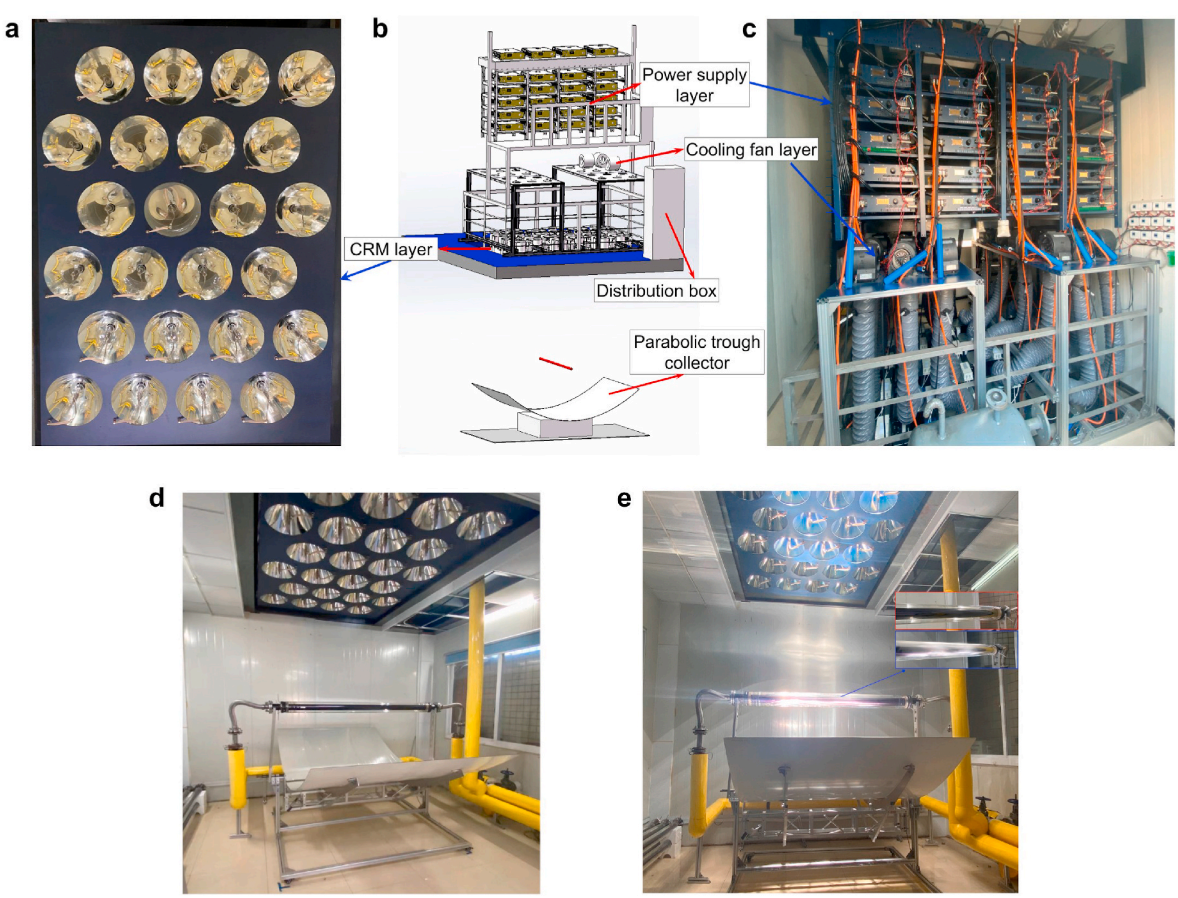

Fig. 6. (a) Photograph of the SMCSS. **(b)** Design diagram of the SMCSS. **(c)** Each CRM was equipped with a separate power supply and cooling fan. **(d)** Solar simulator and parabolic trough collector. (**e**) Parts of CRMs are operating, and the inset compares the absorber when the simulator is on (blue frame) or off (red frame).

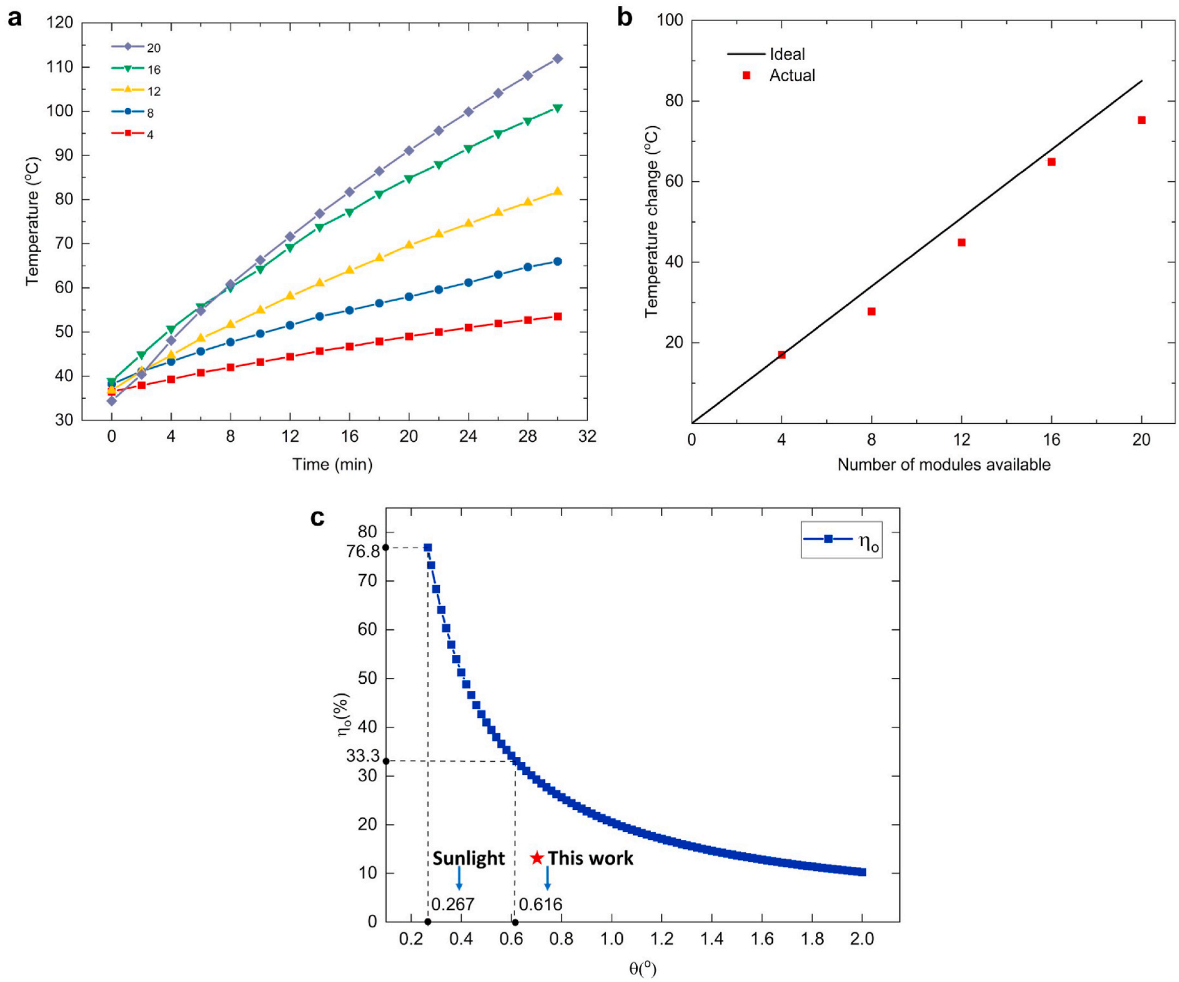

Fig. 7. When 2, 4, 8, 12, 16, and 20 CRMs in the SMCSS are operating, **(a)** the temperature of the thermal oil changes with time, and **(b)** the total temperature change of the thermal oil within 30 min. **(c)** Optical efficiency ($\boldsymbol{\eta_o}$) change of the parabolic trough collector with the HDA (θ) of light.

determined to be less than 1°, which is achieved for the first time in CRMs and is also the state-of-the-art level even compared to CSSs with AOMs. As shown in Table 3, when the diameters of both surface A and surface B were set to 200 mm and the corresponding θ was 0°, the optical power on surface A was significantly less than that on surface B for all four CRMs. This is because a large amount of light on the edge of surface B did not reach surface A after a 1.2-m propagation, which is consistent with our speculation. When reducing the diameter of surface B to 160 mm and θ corresponding to 0.995°, the difference in optical power on the two surfaces is less than 5 %. Therefore, θ_u is 0.995° for the four CRMs, and it can be determined that the light HDA within a 200 mm diameter spot (surface A) is less than 0.955°.

The simulation result in Fig. 4b was also proved by the measurement result. CRM with a Gaussian-like distribution, such as #4, did show better collimation than CRM with a platform area, which was reflected in that CRM #4 had larger radiation in the high collimation area (HDA< 1°). For example, the optical power of CRM #4 on surface A (515.3 W) is higher than that of CRM #1 (400.3 W) and #2 (412.0 W) (Table 3).

Lastly, it is necessary to prove that the light closer to the center of the spot has better collimation, which is one of the foundations of our measurement method. It was demonstrated by proving that θ_e decreases with the reduction of the spot diameter. We demonstrated this from both positive and negative perspectives. On the one hand, we proved that θ_e constantly reduces with the diameter of surface A decreasing (Supplementary Table 1). On the other hand, we also determined that the θ_e became larger (1.43°) when the diameter of surface A was expanded to 240 mm (Supplementary Table 2).

3. Large-scale single-module collimating solar simulator (SMCSS)

With the superior HDA, uniformity, and repeatability of CRMs, large-scale SMCSS can be modularly constructed. We built a large-scale SMCSS with 24 CRMs (Fig. 6a–c) with CRM #1 as the template (Fig. 5a), and it was used in a 2.55 m × 1.57 m parabolic trough solar collector (Fig. 6d and e) that included a thermal oil circulation system (parameters can be seen in Supplementary Table 3).

3.1. Light concentration experiments and collimation of the SMCSS

We studied the collimation and uniformity of the SMCSS with light-concentrating experiments and simulations. In the experiments, the power of each CRM was set to 2.7 kW, and the initial flow rate of thermal oil was controlled at 4.70 ± 0.1 m^3/h. We opened different amounts of CRMs in the experiments and kept operating CRMs symmetrically distributed on both sides of the absorber. It can be seen that the temperature of the thermal oil significantly increased within 30 min (Fig. 7a). But the temperature rising rate decreased when the temperature increased because of the higher heat loss. The temperature change within 30 min showed a nearly linear relationship with the number of operating CRMs (Fig. 7b), indicating that the radiation output of the SMCSS exhibits a nearly linear relationship with the number of

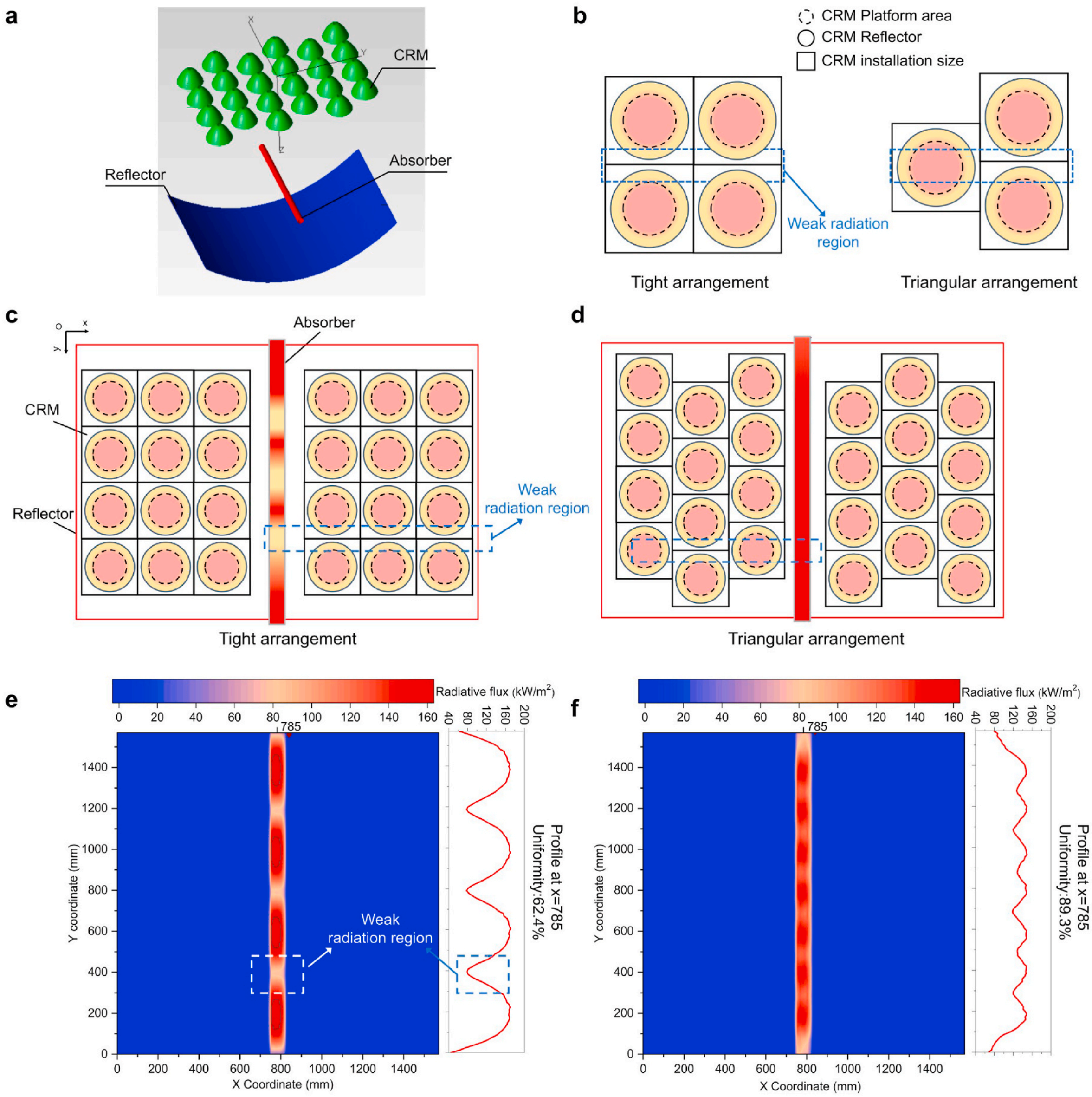

Fig. 8. (a) Model of the SMCSS and parabolic trough collector in the MRCT simulation. **(b)** Two arrangement principles of CRMs: tight arrangement and triangular arrangement; the black box, black circle, and dashed circle represent the installation size, reflector, and platform area of CRMs, respectively. **(c)** Tight arrangement scheme and **(e)** corresponding simulation result of radiation distribution on the absorber and profile of radiation at X = 785 mm. **(d)** Triangular arrangement scheme and **(f)** corresponding simulation result of radiation distribution on the absorber and profile of radiation at X = 785 mm.

operating CRMs because of the excellent repeatability of the CRMs. This ensures that the actual radiation area of the SMCSS can be controlled by opening different numbers of CRMs.

The optical efficiency (η_o, the ratio of the radiation collected by the absorber to the radiation incident on the collector) was calculated as 33.3 % (Supplementary Note 5) from the light-concentrating experiments. The HDA of the SMCSS can be estimated to be 0.616° by the functional relationship between the HDA and the optical efficiency of the parabolic trough collector [22] (Fig. 7c, Supplementary Note 6). This result is close to the measurement result of the single CRM (θ <0.955°). The reason the result is slightly less than the θ_u of the CRM (0.955°) is that the HDA measured by the light-concentrating experiment reflects the collimation of the overall light within the spot instead of only light on the edge, which is consistent with the definition of the θ_u (upper limit of the light HDA within the spot).

3.2. Uniformity of the SMCSS

The uniformity of CSS ensures to replicate of the distribution produced by natural sunlight on the absorber. For instance, in linear concentrating devices like parabolic trough collectors, the radiation distribution along the central axis of the absorber is uniform. In point concentrating devices, the distribution follows a series of concentric circles on the absorber. By appropriately designing the arrangement of CRMs, the SMCSS can effectively simulate these characteristic features.

Specifically, we noticed that the platform area is less than the area of the reflector when CRMs take CRM #1 as the template (Fig. 8b). Therefore, there must be a weak radiation area between spots when CRMs adopt the tight arrangement (Fig. 8b), and there will be a corresponding weak radiation gap when the spots are focused on the absorber (Fig. 8c). The simulation (Supplementary Note 1) proves that the layout designed by the tight arrangement results in a uniformity of only 62.4 % on the absorber along the central axis (Fig. 8e). There are three weak radiation areas and four intense radiation areas on the absorber, which

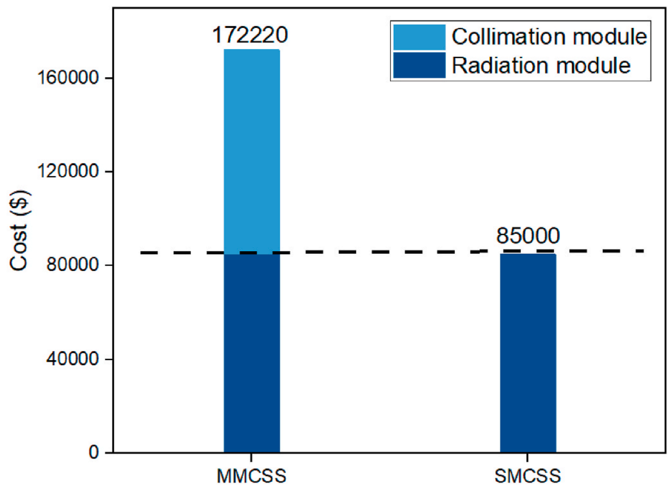

Fig. 9. Cost comparison of the SMCSS and MMCSS with the same radiation area of 2.55 m × 1.57 m. The cost of SMCSS only includes the cost of CRMs, and the cost of MMCSS contains the cost of radiation modules, homogenization modules, and collimation modules.

is far more uneven than the radiation generated by natural sunlight. However, we found that a triangular arrangement principle can solve this problem, in which the third CRM can fill the radiation gap between two CRMs (Fig. 8b). Simulation results confirmed that the scheme designed by the triangular arrangement (Fig. 8d) ensured an even radiation distribution with a uniformity of 89.3 % along the direction of the central axis (Fig. 8f), which well simulated the radiation distribution on the absorber under natural sunlight.

Nevertheless, despite the excellent simulation of the radiation distribution on the absorber, our testing process revealed a relatively poor uniformity of the SMCSS compared to CSS with AOMs, primarily due to its modular feature. We can see the shape of spots of individual CRMs in the radiation area of the SMCSS (Supplementary Fig. 6), and there are some weak radiation areas among these spots. Hence, it becomes imperative to ascertain the potential of the SMCSS to produce uniform radiation like natural sunlight. In our preliminary investigations, we have provided initial evidence that achieving such uniform radiation is indeed feasible. This is attributed to the great flexibility of adjusting the radiation distribution of a single CRM and the layout of the CRMs. We also proposed a scheme and demonstrated that it could produce uniform radiation with simulation (Supplementary Note 7, Supplementary Figs. 7–8). However, a more general scheme required further exploration and implementation.

3.3. Energy efficiency and cost advantage of the SMCSS

The SMCSS achieved an energy efficiency of 31.6 % (Supplementary Note 8), which is nearly twice the most advanced efficiency of CSSs in the past (Table 1). The high efficiency is mainly due to the elimination of the homogenization module and collimation module and the corresponding light absorption and attenuation effects compared to the multi-module collimating solar simulator (MMCSS). The high energy efficiency allows lamps with lower power to be used in the SMCSS, which is beneficial for increasing the reliability and security of the system. On the other hand, high-power lamps (still lower compared to lamps in CSS with AOMs) can be used to achieve high-flux collimated light in the SMCSS. For example, we used xenon lamps of 3 kW to achieve collimated radiation larger than 10 kW/m^2 in this work. Combining both high collimation and high flux, the high-flux SMCSS can simulate sunlight with an area larger than its own radiation area. This magnification effect is significantly meaningful for further decreasing the cost of CSS and saving experimental space (Supplementary Note 8).

We calculated the cost of the SMCSS and the MMCSS with the same radiation area and found that the cost of the SMCSS decreased by 50.6 % compared to the MMCSS (Fig. 9). We thought that the decrease in cost is primarily from the elimination of collimation modules in the SMCSS. The conclusion is based on two estimations in the calculation: 1) We ignored the cost of the homogenization module in the MMCSS since it is relatively low compared to the radiation module and collimation module, although this is an underestimation of the cost of MMCSS. 2) We set the radiation modules of the MMCSS to have the same cost as the CRMs in the SMCSS (85,000 $ which is calculated based on our actual procurement price) based on our market investigation. The logic behind this estimation is that the MMCSS can save a part of the cost in radiation modules because the requirement for the precision of parts is lower than CRMs, but higher-power lamps (Table 1) and matching cooling systems are necessary for the MMCSS because of its lower energy efficiency, which brings an increase in cost compared to the SMCSS. The impact of these two factors on prices basically offsets each other.

Therefore, an accurate estimation of the cost of the collimation modules in the MMCSS is essential. It should be noted that a collimation module with such an area of 2.55 m × 1.57 m cannot be found directly in the market, which reflects the manufacturing dilemma of the large-scale MMCSS to a certain extent. Hence, we estimated the cost based on small collimating mirrors now that the large-area collimating module is generally manufactured by splicing hundreds of smaller mirrors. To ensure the strictness of the estimation, we calculated the cost with six kinds of small collimating mirrors of different sizes. The cost in different cases was at a similar level of 80,000 $ - 280,000 $, which proved the reliability of the estimation. We chose the lowest price of 87,220 $ in all cases as the final result. We should note that the cost of collimating modules may still be undervalued. This and some other details of cost calculation can be seen in Supplementary Note 9.

The great decrease in cost makes the promotion of large-scale CSS more feasible. Moreover, the decreased proportion of the cost will be larger with the increasing radiation area of the solar simulator because the cost of SMCSS increases linearly with the radiation area, but that of the MMCSS grows superlinearly because of the existence of the large-scale collimation module.

4. Conclusion

We have successfully developed CRMs capable of directly producing uniformly collimated light with an HDA of less than 0.955° without assistance from AOMs. To the best of our knowledge, this is the first time CRM has accomplished an HDA of less than 1°, which is a state-of-the-art level even compared to CSSs with AOMs. The CRM was accomplished by conducting a detailed analysis of the deviation between the ideal model and the actual CRM. Then we used the high-precision light source and parabolic reflector, and a high-resolution three-dimensional adjustment method to eliminate these deviations and realize the idealized geometric optical model.

It was proved that The CRMs can modularly build large-scale SMCSSs because of their excellent repeatability and the simple template adjustment method we developed. By employing 24 CRMs, an SMCSS with a radiation area of 2.55 m × 1.57 m was constructed. Light-concentrating experiments on a parabolic trough solar collector demonstrated its excellent collimation consistent with the single CRM. We also proved that the SMCSS could provide an excellent simulation of the radiation distribution generated by natural sunlight on absorbers. Additionally, due to the elimination of AOMs, the SMCSS demonstrates a remarkable reduction in costs by 50.6 %, and a record-breaking energy efficiency surpassing 30 %, almost twice the previous CSS energy efficiency record.

In summary, the CRM and SMCSS exempt the use of AOMs, which significantly decreases the construction threshold of large-scale CSS from both system complexity and cost. This advancement holds tremendous promise for diverse experimental scenarios requiring large-area collimated light and serves as a catalyst for advancing the application of large-scale CSSs in civilian solar research.

CRediT authorship contribution statement

Yuan Gao: Conceptualization, Methodology, Validation, Resources, Writing – original draft, Writing – review & editing. **Xuan Zhu:** Methodology, Validation, Resources. **Jiangfeng Chen:** Validation, Resources, Visualization. **Yin Xie:** Validation, Resources, Visualization. **Jianan Hong:** Validation, Resources. **Junyu Jin:** Validation, Visualization. **Junchou Han:** Resources, Visualization. **Xuhan Zhang:** Validation, Resources. **Chenyu Xu:** Conceptualization, Methodology, Validation, Resources, Writing – review & editing. **Yanwei Zhang:** Conceptualization, Methodology, Resources, Writing – review & editing, Supervision.

Declaration of competing interest

We have no conflicts of interest to disclose.

Acknowledgments

This work was financially supported by National Natural Science Foundation of China (51976190), Zhejiang Provincial Natural Science Foundation of China under Grant No. LDT23E06014E06, and Fundamental Research Funds for the Central Universities(2022ZFJH04). The authors gratefully acknowledge this support.

The electrical and mechanical systems were provided by Shanghai Fode Lighting Equipment Co., Ltd., China.

Appendix A. Supplementary data

Supplementary data to this article can be found online at https://doi.org/10.1016/j.renene.2023.119675.

References

[1] M. Nakakura, M. Ohtake, K. Matsubara, K. Yoshida, H.S. Cho, T. Kodama, et al., Development of a receiver evaluation system using 30 kWth point concentration solar simulator, Energy Proc. 69 (2015) 497–505.
[2] W. Wang, L. Aichmayer, J. Garrido, B. Laumert, Development of a Fresnel lens based high-flux solar simulator, Sol. Energy 144 (2017) 436–444.
[3] L. Martínez-Manuel, M.I. Peña-Cruz, M. Villa-Medina, C. Ojeda-Bernal, M. Prado-Zermeño, I. Prado-Zermeño, et al., A 17.5 kWel high flux solar simulator with controllable flux-spot capabilities: design and validation study, Sol. Energy 170 (2018) 807–819.
[4] Q. Zhu, Y. Xuan, X. Liu, L. Yang, W. Lian, J. Zhang, A 130 kWe solar simulator with tunable ultra-high flux and characterization using direct multiple lamps mapping, Appl. Energy 270 (2020), 115165.
[5] J. Fang, Q. Liu, S. Guo, J. Lei, H. Jin, Spanning solar spectrum: a combined photochemical and thermochemical process for solar energy storage, Appl. Energy 247 (2019) 116–126.
[6] Q. Liu, H. Hong, J. Yuan, H. Jin, R. Cai, Experimental investigation of hydrogen production integrated methanol steam reforming with middle-temperature solar thermal energy, Appl. Energy 86 (2009) 155–162.
[7] J. Sui, Q. Liu, J. Dang, D. Guo, H. Jin, J. Ji, Experimental investigation of methanol decomposition with mid- and low-temperature solar thermal energy, Int. J. Energy Res. 35 (2011) 61–67.
[8] T. Sebastian, S. Jakob, B. Søren, Electrified methane reforming: a compact approach to greener industrial hydrogen production, Science 364 (2019) 756–759.
[9] Y. Liu, P. Hu, Q. Zhang, Z. Chen, Thermodynamic and optical analysis for a CPV/T hybrid system with beam splitter and fully tracked linear Fresnel reflector concentrator utilizing sloped panels, Sol. Energy 103 (2014) 191–199.
[10] Z.-D. Cheng, Y.-L. He, K. Wang, B.-C. Du, F.Q. Cui, A detailed parameter study on the comprehensive characteristics and performance of a parabolic trough solar collector system, Appl. Therm. Eng. 63 (2014) 278–289.
[11] L. Valenzuela, R. López-Martín, E. Zarza, Optical and thermal performance of large-size parabolic-trough solar collectors from outdoor experiments: a test method and a case study, Energy 70 (2014) 456–464.
[12] X. Dong, G.J. Nathan, Z. Sun, P.J. Ashman, D. Gu, Secondary concentrators to achieve high flux radiation with metal halide solar simulators, J. Sol. Energy Eng. 138 (4) (2016), 041001.
[13] D. Rodriguez-Sanchez, G. Rosengarten, Improving the concentration ratio of parabolic troughs using a second-stage flat mirror, Appl. Energy 159 (2015) 620–632.
[14] N. Thomas, T. Beck, S. Chakraborty, M. Gerber, S. Graf, D. Piazza, et al., A wide-beam continuous solar simulator for simulating the solar flux at the orbit of Mercury, Meas. Sci. Technol. 22 (2011), 065903.
[15] O.G. Feil, H.U. Frey, Solar Simulation with a Rectangular Beam, 15th Space Simulation Conference, 1988, pp. 278–288.
[16] R.E. Bartera, H.N. Riise, C.G. Miller, Solar simulators at the Jet propulsion laboratory, Appl. Opt. 9 (5) (1970) 1068–1074.
[17] J. Jin, Y. Hao, H. Jin, A universal solar simulator for focused and quasi-collimated beams, Appl. Energy 235 (2019) 1266–1276.
[18] S.P. Kenny, J.H. Davidson, Design of a multiple-lamp large-scale solar simulator, J. Sol. Energy Eng. 116 (4) (1994) 200–205.
[19] Ł. Bartela, B. Stanek, D. Węcel, A. Skorek-Osikowska, A solar simulator numerical modeling for heat absorption phenomenon research in a parabolic trough collector, Int. J. Energy Res. 46 (2022) 10074–10087.
[20] https://www.osram.com.cn/cb/. (Accessed 12 March 2023).
[21] https://www.optiforms.com/. (Accessed 12 March 2023).
[22] A. Rabl, Comparison of solar concentrators, Sol. Energy 18 (1976) 93–111.